Title

Engineering an elastic bioink for 3D Bioprinting of the Urethra

Author

Booth, Daniel Thomas

Publication Date

2022

Peer reviewed|Thesis/dissertation

UNIVERSITY OF CALIFORNIA

Los Angeles

Engineering an elastic bioink for 3D Bioprinting of the Urethra

A thesis submitted in partial satisfaction

of the requirements for the degree Master of Science

in Chemical Engineering

by

Daniel Thomas Booth

2022

ABSTRACT OF THE THESIS

Engineering an elastic bioink for 3D Bioprinting of the Urethra

2022

by

Daniel Thomas Booth

Master of Science in Chemical Engineering

University of California, Los Angeles

2022

Professor Nasim Annabi, Chair

There stands considerable opportunity in the medical field for the rapidly expanding scope of additive manufacturing technology such as 3D bioprinting, as the capacity for fabricating patient-unique tissue engineered scaffolds in a rapid, direct manner may expand the availability and applicability of surgical techniques. In this work, a 3D bioprinting technique was used to fabricate tubularized constructs for the urethral tissue regeneration. In particular, an elastic hydrogel-based biomaterials were optimized to be used as bioinks for 3D bioprinting of a construct for urethral reconstruction. Two radially distinct regions were determined to be necessary for this tissue-engineered construct, to provide cellular proliferation and structural support to the graft while de-

facto partitioning two distinctive tissue regions in the urethra, one made of gelatin methacryloyl (GelMA) for the urothelium, and another layer made of methacrylated elastin-like polypeptide (mELP) and GelMA for smooth muscle cells (SMCs). GelMA and mELP were selected for the hydrogel blend to ensure mechanical durability while attaining a greater extensibility desirable for the urethral tissue region. Chemical characterization via H-NMR analysis provided evidence of the photocrosslinking mechanism which was utilized to crosslink the bioink and solidify the construct with the degree of crosslinking as 55% for GelMA and 68% for mELP/GelMA. Mechanical characterization allowed us to select an optimal ratio of GelMA/mELP and achieve the mechanical properties close to native urethra. Following this stage, the optimization of printing parameters for each bioinks yielded for temperature 30 and 8 °C, printing speed of 8 mm/s and 5 mm/s, and extrusion pressure 4 psi and 15 psi for the 10% (w/v) GelMA bioink and 15% (w/v) 1:1 mELP/GelMA bioink, respectively. Future studies will focus on *in vitro* cellular studies to ascertain the cytocompatibility of this material, as well as quantify the construct's efficacy in future applications surgically.

The thesis of Daniel Thomas Booth is approved.

Irene Chen

Renea Sturm

Nasim Annabi, Committee Chair

University of California, Los Angeles

2022

TABLE OF CONTENTS

LIST OF FIGURES

ACKNOWLEDGEMENTS

The completion of this thesis is a major milestone in my career and my life, and I owe so much thanks to those supporting me through this work. I could not have done this without the love, care, and generosity of many, and for that I am humbled and grateful.

Thanks to Dr Nasim Annabi for accepting me as a Masters student in her lab, and for giving me so much opportunity. Thanks to Dr Renea Sturm as well for her invaluable guidance through the project.

Thanks to Dr Mahsa Ghovvati and Saumya Jain for their friendship in the lab. Thanks to Avijit, Mahsa, and Ronak for their valuable collaboration in this work. Thanks to all my fellow lab members for the camaraderie these past two years.

Thanks to my parents Thomas Booth and Betty Boyadjian, who have guided me by example on not only how to work hard in life but also focus on what really matters. Thanks to my brother Alex for his lifelong friendship, and to our dog Teddy for being a very good boy.

Thanks to my friends Adam Keppler, Farhan Saleh, Erik Najera, Richard Umboh, and Adam Turken for helping me compartmentalize and excel.

Thanks most of all to Michelle, who has been by my side every day, and who inspires me to be more selfless.

CHAPTER 1: Introduction

3D bioprinting's versatility as a technology has expanded in scope across the medical industry, particular regarding applications in urology. Demand for tubular grafts developed for reconstructive operations represents a sizable topic within this specialty, and the programmable and repeatable fabrication features of 3D bioprinting is well situated to answer these demands. Here we summarize recent developments for the 3D bioprinting of the urethra, assessing and comparing the merits of the varied bioprinting methods as well as other means of fabrication. Further technological advancements in bioprinting pave the way to clinical use of fabricated patient-specific urethral constructs, from techniques already being designed for urethral reconstruction to specialized printers that possess unique fabrication advantages.

1.1 Background & Clinical Need

Mass production has played an undeniable role increasing the length and quality of life across vast regions of the globe in recent centuries, as all manner of products become more widely available and affordable. This extends to the medical industries as well, where the mass fabrication of medical devices and treatments assist the preservation of life more widely than ever before. Despite these benefits, a longstanding limitation of mass production of medical devices was the sacrifice of personalized medical devices and constructs. Recently in the realm of polymer-based constructs, this barrier has begun to evaporate, as unique 3D structures can be generated through the advent of stereolithography, an established technique, utilizing ultraviolet light to harden polymer layers from a liquid bath to form complex 3D structures [1]. Since then, newer techniques in rapid prototyping have continued to optimize the ease with which tissue constructs could be generated. 3D bioprinting is one such technique and is an emergent tissue engineering strategy.

For an anatomy as disparate between patients as the urethra, bioprinting's affinity producing cellular constructs supported by hydrogel matrices and aptitude in personalizing these constructs presents unique opportunities for innovation.

In the medical industry, 3D printing has already emerged as a method of fabricating prosthetics [2], surgical implants [3], instruments [4,5], and pharmaceutical products [6]. 3D printing is a form of additive manufacturing (AM), which in comparison with the other two techniques of manufacturing (formative and subtractive) is best for low quantity production of high-resolution designs; this is because limitless geometric part designs can be produced via AM [7]. Bioprinting processes typically involve three distinct stages (respectively known as pre-bioprinting, bioprinting, and post-bioprinting using live cells. In pre-bioprinting, a 3D rendering of the desired scaffold is developed, conventionally through computational tomography (CT) or magnetic resonance imaging (MRI). Cells taken from biopsy or selected from a relevant cell line are also isolated and expanded. Next these cells are incorporated with hydrogels to serve as the supportive matrix in a bioink, with supplementary nutrients or sacrificial materials added depending on the bioprinting method. The bioink is then printed according to the selected method of bioprinting to from a 3D construct. Lastly, in post-bioprinting the printed construct is cultured in conditions conducive to maintaining stable structure and cellular proliferation [8].

Applying 3D bioprinting towards urological tissue constructs is promising due to the need for personalized grafts compatible with the unique patient anatomies in the lower urinary tract. Bioprinting applications in the spongy or penile urethra, which travels the length of the penis via the corpus spongiosum, is a relatively understudied area, which possesses an unmet clinical need for tissue engineered constructs [9]. This relativity is due in part to the variability that emerges between patients in these regions; further, the urethral tubing has varied lumenar histology along

its length. Reconstructing damaged regions of these tissues with CT or MRI generated scans with a bioprinter could expand the native mimicry of tissue grafts/constructs and improve healing efficacy. A literature search on this topic in PubMed yielded less than a dozen articles using keywords 'bioprinting' and 'urethra' since 2016, with few more appearing when adding 'bladder' to the query. While this belies the relatively understudied nature of urethral bioprinting, in this chapter, recent advances on the use of 3D bioprinted tissue constructs as alternatives to autologously sourced grafts are highlighted.

Urethroplasty is a reconstructive treatment for urethral defects, with the most common being secondary to traumatic, infectious, or congenital conditions. Hypospadias is a common congenital deformity, arising in an estimated 7000 boys born in the United States annually. The majority of boys undergo surgical correction, with overall private insurer expenditures for corrective procedures within the first three years of life approximately $8,000 USD per child (circa 2013) [10]. Proximal hypospadias repairs have frequent surgical complications following reconstructive surgery, with re-operation occurring in 49-68% [11-13]. Urethral stricture, a narrowing of the urethral lumen, is more commonly observed as the need for urethroplasty in adults due to traumatic injury, infection, or radiation exposure. An estimated 200,000 patient visits per year account for urethral stricture in the U.S., with associated care costs of nearly $200 million [10].

When extensive or in the setting of abnormal tissue, a secondary tissue source may be required during urethra repairs. The current tissue sources for these grafts are preputial (foreskin) or buccal (superficial inner cheek) [14]. Figure 1 demonstrates a buccal graft harvest, represented with a cartoon schematic (Figure 1A-B). These grafts once tubularized are applied to the ventral penile surface and sutured to the adjoining urethra (Figure 1C-F). Images of both surgical steps

are also included for reference (Figure 1G-K). However, these autologous tissue sources can be limited by inadequate tissue and can result in donor site morbidity, such as contracture or effects on salivation or sensation [15]. Additionally, these tissues fail to recapitulate the unique elastic properties of the urethral lumen, which undergoes considerable mechanical stress and must be capable of frequent radial expansion and contraction according to the natural excretion of urine from the body as well as longitudinal extensibility during penile erection. Further, while tubularized grafts of harvested tissue assist in reconstruction and healing, they do not recapture the layers & folds of the lumenar surface. Also, the success rates for the surgical repair of proximal hypospadias mentioned is particularly striking in statistics surrounding urological procedures involving graft insertion. The complex, atypical anatomies of patients diagnosed with disorders of sex development (DSD) positively associate with inhibited efficiency of healing with autologous grafts [16]. Positive associations were also observed for older age at the time of a proximal hypospadias repair, with patients diagnosed with DSD being more likely to undergo unplanned reoperation within the first two years of repair [17]. A promising alternative to the autologous methods of graft fabrication is urethral tissue engineering, both to minimize donor site morbidity and create a structural replacement that more closely approximates urethral tissue functionality. This chapter will address the recent investigations made into the subject of bioprinted urethral constructs as well as other forms of alternative graft synthesis, comparing the advantages of printing methods and the future directions of the field.

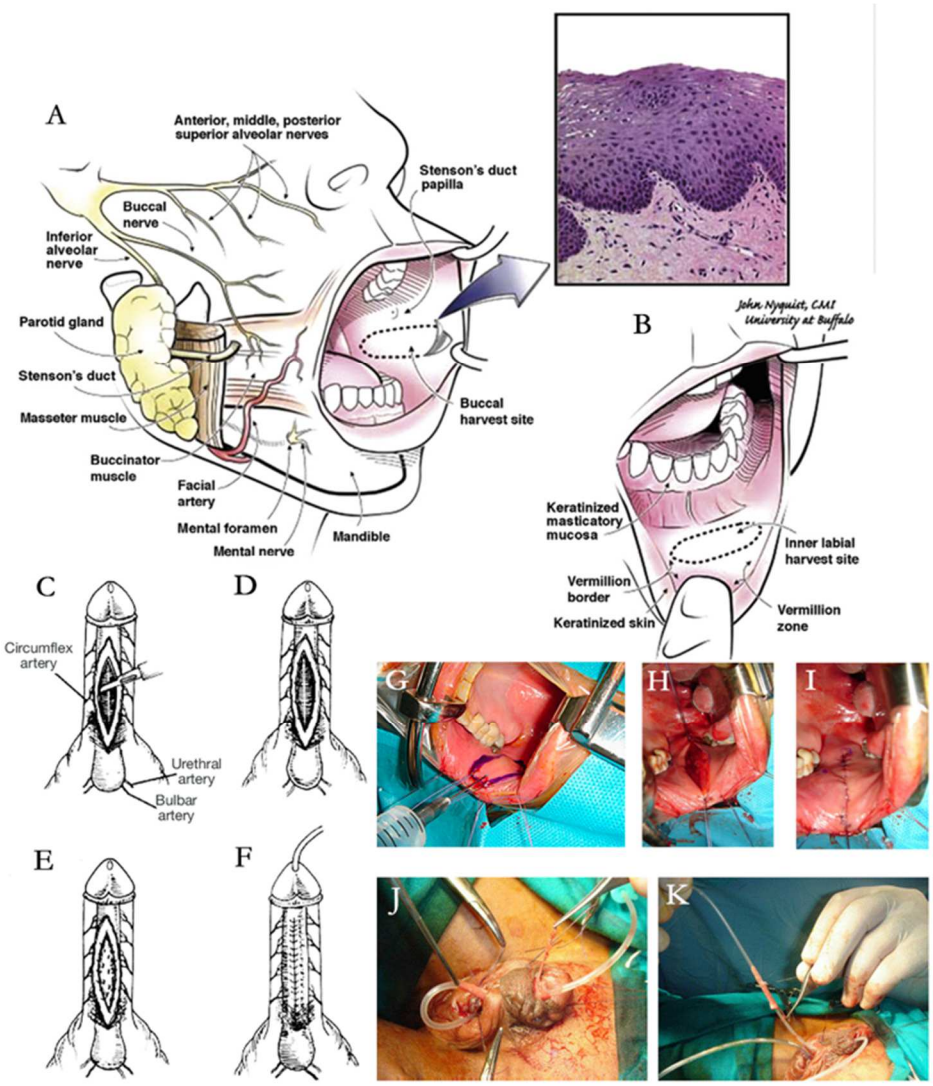

Figure 1. Representative depiction of buccal mucosa graft harvest and urethroplasty. (A) Buccal mucosa harvest site displaying anatomical landmarks, with photomicrographic image of buccal mucosa tissue. (B) Labial mucosa harvest site with associated anatomical landmarks. Reproduced with permission [54]. Copyright Elsevier, 2007. Stages of a dorsal inlay urethroplasty, beginning with incision at the shaft of the penis (C) and smooth muscle layer (D), exposure of innermost fascia (E), insertion of implant (F). Reproduced with permission [55].

Copyright Elsevier, 2006. Harvesting of buccal mucosa, with demarking sacrificial site (G), excising tissue (H), and suturing over (I). Insertion of autologous scaffold, with threading on the tubularized scaffold (J), and insertion (K). Reproduced with Permission [14] Copyright 2010, Elsevier.

1.2 Methods of Bioprinting Fabrication

3D bioprinting has distinct potential for engineering synthetic urethral tissue and presents a solution to the abundant need at present. Problems with current tubularized grafts stem in many respects from an inability to recapture the diversified layers and highly extensible properties of the native tissue therein. 3D bioprinted constructs shaped in replication of scanned patient anatomy may be specifically beneficial in this regard. Printer bioinks are primarily composed of hydrogels, allowing for easy variation in construct geometry as the matrix can be assembled post-printing via crosslinking reactions. Further, in 3D bioprinting a vast array of hydrogels and proteins can be used as bioinks, providing opportunity for the selection of materials desirable for specific mechanical properties. 3D bioprinted constructs can thus be engineered with materials appropriate for the mimicry of urethral tissue mechanics. While some bioprinting methods have already been applied towards the fabrication of urethral constructs, others have yet to delve past more common tubular structures. However, each technique possessing grounds for innovation in urethral tissue engineering, as each bears advantages and limitations where novel study can improve the urethral construct's efficacy. Figure 2 below presents a conceptual representation of various bioprinting techniques.

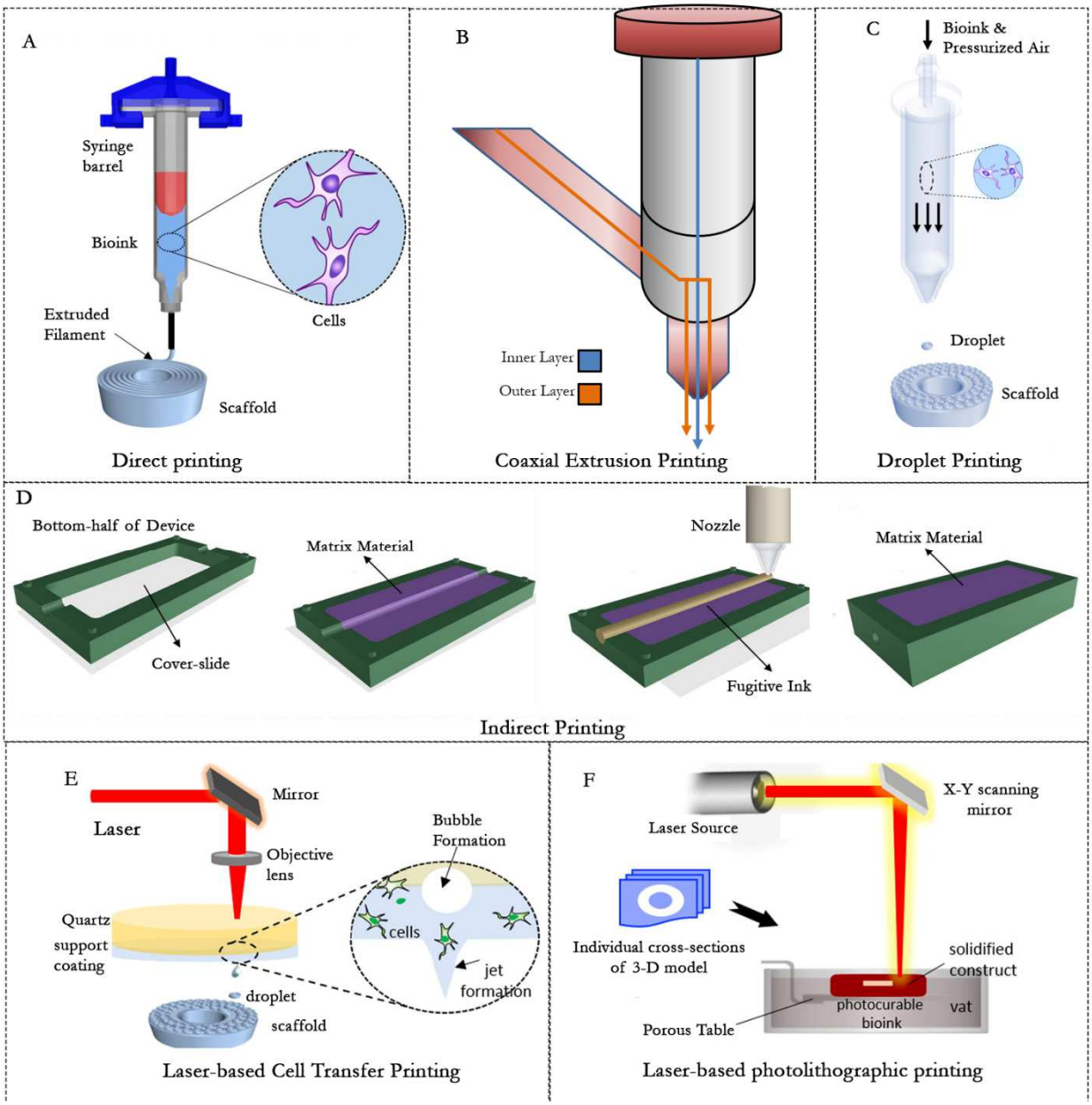

Figure 2. Common Methods of 3D bioprinting. (A) Direct Inkjet-based printing (B) Coaxial Extrusion (C) Droplet-based printing (D) Indirect inkjet-based printing (E) Laser-based forward transfer printing (F) Laser-based photolithographic printing. Reproduced with permission [53]. Copyright 2017, Elsevier.

Urethral scaffolds have often been designed with two regions separated radially to coincide with the urothelial cellular layer and the external smooth muscle layer [19-21]. Reasons behind this radial partition are twofold, residing from standpoints both on a cellular and structural basis. Smooth muscle cells (SMCs) compose the external region of the urethra, while in the interior the urothelium layers are subdivided into umbrella, intermediate, and basal cells [18]. Functionally, this provides the urethra with diffusive and immune control in the urothelium, while SMCs externally locomote the automatic muscle movements responsible for urination, a process known as peristalsis. Bioprinted urethral constructs thus require a distinct separation between the lumen and outer circumference where distinctive cell layers can be observed.

1.2.1 Coaxial Extrusion & Direct Bioprinting of Urethral Tissue

Recently, studies using 3D bioprinting to produce cellularized tubular urethra have most commonly utilized coaxial-nozzle printers (Figure 2B). This method of bioprinting has been the first with significant attempts at such a construct due to their affinity producing multilayer constructs in a single step. Zhang *et al.* produced tubular poly(ε-caprolactone) (PCL)/poly(lactide-co-caprolactone) (PLCL) scaffolds capable of mimicking the structure and mechanical properties of native male rabbit urethral tissue [19]. A variation on a classical tubular geometry through the incorporation of a helical 'ribbing' improved the stretchability and elastic modulus of the construct (Figure 3). Introducing the helical ribbing in the designed PCL/PLCL scaffold enhanced stretchability while columnar designs improved tensile strength. Techniques such as these may assist in closing the gap between the mechanics of native tissue and synthetic scaffolds. However, the robust PCL backbone of the structure could not support cellular proliferation, and thus fibrin hydrogel was incorporated to inlay urothelial cells and SMCs. Similarly, Ouyang *et al.* utilized a

coaxial extrusion technique, involving an *in-situ* crosslinking strategy whereby a light-permeable capillary enabled defined structural formulations while retaining good cellular viability [20]. Their methodology utilized GelMA and poly (ethylene glycol) diacrylate (PEGDA) and can be extended to broader 3D bioprinting applications designed around photo-initiated crosslinking during bioink extrusion. In addition, their extrusion system provides the means for multilayer structures, though these structures are cylindrical in geometry rather than tubular. Pi *et al.* designed a multichannel coaxial extrusion system using a blend of GelMA, eight-arm poly(ethylene glycol) (PEGOA), and alginate, capable of developing long segments of tubular constructs with controlled layer deposition [21]. Human primary bladder smooth muscle cells (hBdSMCs) and urothelial cells both displayed high construct biocompatibility within their respective layers, and distinct boundaries for the tubular structures were maintained.

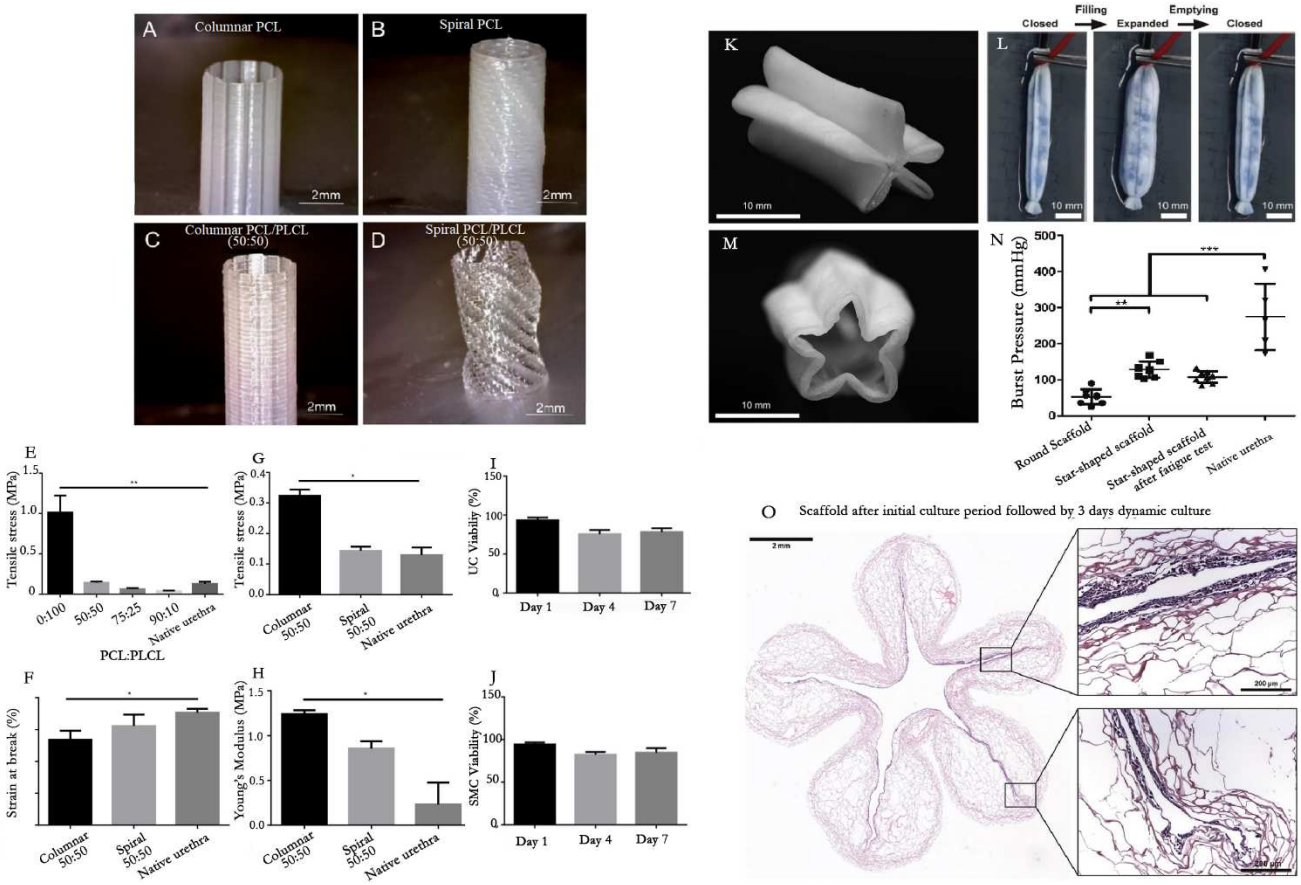

Figure 3. Bioprinted constructs of male New Zealand rabbit urethra with structural modification to tubularized design. (A) PCL scaffold with columnar design. (B) PCL scaffold with spiral design. (C) PCL/PLCL (50:50) scaffold with columnar design. (D) PCL/PLCL (50:50) scaffold with spiral design. Mechanical testing of various PCL/PLCL scaffolds, with tensile stress of varying ratios of PCL/PLCL (E), columnar or spiral tensile strain (F), stress (G), and modulus (H). The quantitative data for cell viability of UCs (I) and SMCs (J) in the bioprinted urethra over time. Reproduced with permission [19]. Copyright 2017, Elsevier. (K/M) Macroscopic view of collagen scaffold in closed and partially open position. (L) Folding and unfolding of scaffold after injection and removal of water. (N) Burst pressure of various scaffold conditions vs. native urethra. (O) H&E staining of cross-sections of cell-seeded star-shaped scaffolds. Reproduced with permission [22]. Copyright 2017, Elsevier.

Direct bioprinting methods utilize pressurized forces to direct the flow of bioink out of the nozzle, creating the shape of printed products without any necessary casting (Figure 2A). Such extrusion methods are simple in experimental execution and allow for the printing of multi-component bioinks containing suspended live cells such that scaffolds can be cultured post-print without requiring further treatment [53]. Versteegden *et al.* used direct bioprinting to create a collagen-based construct, devising a star-shaped tube which expands with lumenal flow [22]. This unique geometry was selected to mimic physiological feature of the spongy urethra and its radial elasticity. Allowing for the expansion of the lumenal cross-sectional area as fluid was excreted, this feature provided control on the hydrodynamic pressures upon urethral tissue of urine flow. Beyond achieving cellular proliferation along the inner construct surface and maintaining its mechanical integrity after cyclic flow, their construct's radial elasticity more closely resembled native tissue behavior than previous designs. Scaffold design overall seemed to benefit from innovative structural techniques to improve the mechanical properties (Figure 3). Designs which

have capacity for radial expansion such as the scaffold by Versteegden *et al*. may improve scaffold's compatibility with native tissue long term, as the regenerated region would less encumber the hydrodynamics of fluid flow and facilitate urethral contraction/expansion.

1.2.2 Indirect, Droplet, and Layer-based Bioprinting of urethral tissue

Similar to direct extrusion, droplet-based techniques deposit the bioink with precision to form printed structures with a non-contact extrusion tip (Figure 2C). Droplet-based bioprinting (DBB) are desirable due to their capacity for replicating the detail of a 3D scan to a high degree of fidelity [27]. Three differing techniques have emerged for droplet-based bioprinting according to the method of extrusion including thermal-, electrostatic-, and piezoelectric-drop on demand [28]. In thermal droplet-based bioprinting, a current generated to a heating medium over precise time intervals creates control over the formation of droplets, the size and rate of which can be tuned in printing. With the piezoelectric–based approach, the current is driven to a piezoelectric actuator, which creates the mechanical stress and induces the locomotion of a small volume of bioink, which coalesces into droplets. Inkjet-based droplet printing pressurizes the bioink suspension at the nozzle tip. Cell survival in droplet-based bioprinting can be affected by disruption to cell membranes or heat spikes caused by the repeated droplet formation, which may affect the cellular proliferation of the printed construct. However, the highly precise degree of control that droplet-based printing offers may provide new avenues to improve the efficacy of urethral constructs and create highly personalized scaffolds for surgical use.

While they have yet to be utilized for urethral tissue, ability to fabricate constructs with precise dimension and definition makes DBB fascinating for potential for urethral tissue engineering applications. At present, 3D bioprinted urethral scaffolds only possess a SMC external

layer and an interior layer for urothelial tissue. However, native urothelium is subdivided into umbrella, intermediate, and basal cells, composing a stratum of individually functional cells rather than a monolayer. Basal cells are smaller, more tightly packed cells next to the basement membrane, and with intermediate cells contain elongated nuclei arranged perpendicularly to the basement membrane. Superficial umbrella cells are larger with abundant cytoplasm and may exhibit multinucleation [29]. While it is challenging to reflect this detail in 3D printed layers with coaxial extrusion or direct printing, being capable of matching native anatomy could vastly improve regenerative capabilities of replacement constructs. The droplet-by-droplet precision of DBB may be the key for engineering urethral scaffolds with high resolution.

Another advanced printing method which promises high control and resolution is the laser-based bioprinting (Figure 2E). Laser-based forward transfer bioprinting is based on the use of a laser beam, photo-stimulating the interface between an energy-absorbing intermediate (such as gold, titanium, etc.) and the bioink, which contains a sacrificial material. This sacrificial 'donor layer' is vaporized under the stimulation of the laser, which generates a high gas pressure propelling the bioink compound towards the printing surface [30]. Laser-based bioprinting is generally characterized by its high resolution in its printed structure with a slower fabrication speed and is an orifice-free droplet-based technique which does not suffer from clogging-related failures with highly viscous biomaterials [31]. Xiong *et al.* have shown the effectiveness of utilizing laser bioprinting for engineering tubular and bifurcated constructs, using an alginate-based bioink to produce layer-by-layer in suspension which can be crosslinked chemically [32]. In this study, the authors present that their hydrogel system's printing resolution can be improved via adjusting the vertical step size when printing. They demonstrated this variation to tune the density of the tubular construct, which has significant histological implications. Though also yet to be applied towards

the urethra, laser-based techniques may be another path to create constructs with a realized stratum of urothelial cells. Where clogging and other complications may arise in DBB due to viscous hydrogels, laser-based approaches have none of these issues. Rather, they face their own complications such as thermal stress due to the laser irradiation, which can alter thermo-sensitive hydrogels and affect the bioink during printing.

Indirect extrusion printing is another method of bioprinting in which the bulk hydrogel contains a considerable quantity of a sacrificial which is removed post printing by thermal or chemical means (Figure 2F). While similar to the direct FRESH approach in the use of a support matrix, indirect extrusion printing distinctly prints about a fugitive ink to create the scaffold structure, whereafter the fugitive ink is separated. Indirect approaches have yet to be utilized towards the lower urinary tract, though they have been used for the fabrication of vascular tissues. For example, Lee *et al.* developed a vasculature network by using an indirect bioprinting technique and sacrificial gelatin to frame hollow collagen fibers [33]. When assessed in conditions operating physiological flow, cellular viability was maintained at 5 million cells/mL density up to 5mm deep into the material. Cellular proliferation was greater in conditions without continuous flow within the hollow tube, as shear forces along the lumenar surface challenged the growing culture. Indirect printing, though not yet seen applied towards urethral tissue, advantageously uses a sacrificial material to support softer materials in printing. Utilizing soft and elastic biomaterials such as elastin-like polypeptides (ELP) may help fabricating constructs mimicking the stretchability of native urethral tissue. However, the soft nature of these materials may cause concern for the feasibility of the printing and handling/suturing of the resulting construct. As urethral tissue engineering continues to develop, indirect bioprinting has potential to play a role in achieving biomimetic physiological and mechanical properties.

Overall, 3D bioprinting is a promising direction for the fabrication of urethral tissue constructs due to its rapidity, relatively inexpensive cost, and ability to accommodate unique patient anatomies.

1.3 Microfabrication of Urethral Tissue Construct Beyond Bioprinting

Advancements in tissue fabrication of the urethra have not just been within bioprinting, as also techniques such as electrospinning or molding have been explored. Table 1 below presents such work developing microfabrication techniques, to provide a whole picture of work produced specifically for the urethra.

Table 1. Microfabrication of 3D urethra tissue

Material	**Method**	**Key Results**	**Experiments *in vivo & in vitro***	**Reference**
Cell-laden PCL/PLCL blend	Direct Bioprinting	•Multilayered cell constructs •Cell viability achieved with fibrin insertion •Biomimetic mechanical properties	*In vitro* NZ White Rabbit bladder UCs & SMCs	Zhang *et al*.
PVA cryogel w/ PLA mold	Fused Deposition modeling	•Geometric, mechanical, and dynamic mimicry of urethra •Use of thermoplastic polyester biomaterial	N/A	Ishii *et al.*
GelMA + Alginate + PEGOA	Coaxial Extrusion	•Multilayered cell constructs •Single step fabrication •Tunable layer printing	*In vitro* Human bladder smooth muscle cells and urothelial cells	Pi *et al.*

PLA copolymer scaffold	Solvent Casting/Particulate leaching	•Stable degradation profile •High porosity with interconnected network •Appropriate cell viability	*In vitro* Adult dermal fibroblasts	Dorati *et al*.
Autologous Tissue	Fused Deposition modeling	•3D-printed anatomical statics & dynamics for posterior urethra	N/A	Joshi *et al*.
Collagen	Direct Bioprinting	•Radial elasticity grants greater fatigue endurance for scaffold	*In vitro* SCaBER cells (ATCC, Manassas, VA, USA)	Versteegden *et al*.
PCL/silk fibroin/collagen	Electrospun	•Good oral mucosal epithelial cell growth •Interconnected porous network & uniform structure, diameter	*In vivo* Oral mucosal epithelial cells, male rabbit subject	Wei *et al*.
PLGA, PLGA/gelatin	Electrospun	•Regeneration of cellular networks near scaffold tips but insufficient in interior •Poor long-term conditions for in vivo subjects	*In vitro* human urothelial cells *In vivo* dozen canine models	Hu *et al.*
PLLA/gelatin	Electrospun	•Upregulated phenotypic expression of seeded cells •Urethral patency and reconstructive modeling *in vivo*	*In vivo* NZ White Rabbit model	Liu *et al*.
PLLA/PEG	Electrospun	•PLLA/PEG scaffolds displayed successful urethral defect repair in target animal study	*In vivo* NZ White Rabbits, scaffolds with hAMSCs	Lv *et al*.

1.3.1 Electrospinning

Electrospinning is an emerging method of building scaffolds through the electronic induction of fiber production, capable of using high voltages to propel charged components of polymer droplets to stretch, drying into spools of fiber along a target surface. Different parameters in electrospinning include the polymer viscosity, polymer concentration, flow rate, and voltage [34]. Standard laboratory approaches to electrospinning utilize spinnerets, often syringe needles, dispensing the polymer solution at a slow feed rate, connected to a power supply emitting high voltages (5-50 kV). Opposite the spinneret and also linked to the power supply is a collection plate, which is conductive to provide a means to complete the circuit by which the electronic forces induce electrospinning [35].

It is significant that fibers in electrospun scaffolds emerge in long-stranded spools, induced by the mobilization of charged regions along the length of the polymer. The hydrogels which compose the skeleton of these scaffolds are thus more ruled by the arrangements & compositions that they naturally compile within their immediate chemical environment. Electrospinning thus has the potential to provide significant mechanical properties to a material that might not be possible with bioprinted constructs. Bioprinted constructs however can successfully culture cells printed directly into the structure, a feature which is impossible for electrospun constructs due to the intense electronic stresses during fabrication [36]. For applications in urethral tissue engineering, distinguishing which advantage offered by each technology is more pertinent can depend on the circumstance. As mechanical performance is rather vital in urethral tissue scaffolds, electrospinning would seem more desirable, but the ability to develop complex layered constructs pre-seeded with region-specific cell lines is hard to ignore. It is our consideration that reflecting the urethra's more complex cell layering with bioprinting technologies is enticing, electrospinning remains an equally viable method in tuning scaffold material properties to simulate native urethra.

Electrospun urethral scaffolds have been tested *in vivo*, with reported successful resumption of function following urethroplasty in animal models. For example, Wei *et al.* inserted an electrospun scaffold composed of PCL, silk fibroin, and collagen into a New Zealand male rabbit model in regions with urethral stricture [37]. The authors seeded their electrospun scaffolds with oral mucosal epithelial cells, observing favorable porosity and cellular proliferation. Cells spread primarily over the surface of the construct rather than diffusing deep into the structure, due to PCL's relatively low favor for proliferation. Similarly, Liu *et al.* observed successful reconstruction in rabbits with an electrospun poly(L-lactic acid) (PLLA)/gelatin construct, showing that their construct maintained urethral patency and facilitated oriented SMC remodeling, lumen epithelialization, and angiogenesis [38]. This is due to the enhanced hydrophilicity and adhesion that gelatin provided in their construct, and as in comparison to scaffolds without gelatin they observed upregulated keratin expression (AE1/AE3) in endothelial cells, actin (α-SMA) in SMCs, and an observed synthesis of elastin. Further, Lv *et al.* observed successful urethral repair in their *in vivo* studies with rabbits using an electrospun scaffold based on PLLA and PEG [39]. However, Hu *et al.* reported poor long-term success in their *in vivo* studies with canine subjects using their electrospun PLGA/gelatin constructs, as urethral strictures and complications involving infection and necrosis occurred in several of their study populations [40].

1.3.2 Molding

Molding is a method of manufacturing wherein the tubular construct is assembled via the knitting of individual membranes of filamentary material, which is used for fabrication of urethral tissue constructs. The individual membranes are usually treated with thermal or compressive pressure, which causes each layer to merge into a desirable composite. Due to the nature of the filamentary

fusing of these constructs, mechanical characteristics can be tuned based on the final application but shaping and seeding the constructs occur separately. However, control over the grain and texture of molded constructs is not as precise, as the material conforms to the mold and gelate spontaneously. Molded samples thus typically take longer to process than bioprinted constructs, as generally the shaping and seeding occur all at once with the printing process. Cell-seeding of molded constructs often requires the acquisition of grafted tissue from a patient source. Sartoneva *et al*. explored the utilization of molding for engineering tubular urethral constructs through the creation of PLA and varied textures of PLCL [41]. They compared the effects of material texture and topography on the mechanical affinity of the constructs, utilizing molding's manufacturing techniques to compare smooth and riveted fibers. While all constructs displayed mechanical stretchability which was favorable, the mechanical stability of smoother textured PLCL was deemed inadequate due to its rapid degradation

Molding techniques have also been explored for the fabrication of compound tubular grafts, which are a mesh of supportive materials is incorporated into an excised native tissue. For example, Jiang *et al*. created a compound of urothelial cells and trypsin/EDTA and observed favorable long-term healing in *in vivo* experiments with NZ white rabbits [42]. Their work evidenced a potential branch in the use of material in urethral scaffold design, as the compound served to reinforce the cellular tissues and provide structural support whereby healing can be ensured. However, the continued necessity of the collection of a patient harvest for such grafts maintains issues observed previously, such as donor site morbidity and loss of function. It is thus molding that represents the most directly transferable method of modifying tubular scaffold generation for urethral healing, even though electrospinning and bioprinting both present significant advantages. While with 3D bioprinting the reconstruction of a damaged urethral region can be achieved directly translating

the topographical contour of a scanned image, with molding a mold of the negative space within the lumen must be generated for the tissue to then be worked into shape. It is just considerable that 3D bioprinting can generate structures similar to molded constructs in fewer, simpler steps.

1.4 Project Outline & Considerations

The project presents a set of hydrogel networks designed for 3D bioprinting a bilayer scaffold for the reconstruction of the spongy urethra, utilizing a polymer blend of GelMA and mELP. We will report the molecular and mechanical characterization of these hydrogel systems, as well as the development of optimized conditions for 3D printing of each respective bioinks. The work presented in this thesis will go on to incorporate *in vitro* cytocompatibility analysis as well as *in vivo* testing to prove the system's expected efficacy in live systems.

GelMA is a functionalized derivative of collagen and a well-studied hydrogel used in a variety of biomaterial applications due to its desirable biocompatibility, ease of synthesis, and low cost [48]. It has been used broadly with a diverse array of co-constituents, capable of being tuned in the presence of other polymers to develop unique hydrogel system properties. Elastin-like polypeptides (ELP) meanwhile exhibit the stretchability desirable for urethral reconstruction, and thus has been incorporated into the bioink. ELP is highly elastic due to its affinity mimicking characteristics of the extracellular matrix (ECM) environment, which is a vital parameter in biological tissue and therefore engineering soft tissues such as skin or blood vessels [43]. However, ELP has previously been shown to be incapable of forming hydrogels independently with stability and mechanical characteristics poor in isolation. Functionalization of ELP with methacryloyl groups increases the degree of crosslinking after its photopolymerization and once it is mixed with GelMA.

As discussed previously, tissue engineering approaches to represent the urethra oftentimes partition the tubular construct radially into regions of urothelial cell networks and those of the SMCs. Similarly, the construct designed for this work was designed in two distinct layers, each with their respective bioink layers (10% (w/v) GelMA for the inner layer, and 7.5% mELP/ 7.5% GelMA (w/v) for the outer layer). For each of these bioinks, GelMA and mELP were both mixed with a photocrosslinking catalyst system composed of Eosin Y, triethylamine (TEA), and vinylcaprolactam (VC). Visible light perturbation at 405 nm instigates the linkage-formation reaction for each system, whereupon the hydrogel expresses gelation and solidifies.

CHAPTER 2: Methods

GelMA synthesis

GelMA was synthesized as described previously [44, 45]. To briefly enumerate this process, 10 g of gelatin from cold-water fish skin or porcine skin (Sigma-Aldrich) was dissolved in 100 mL Dulbecco's phosphate buffered saline (DPBS) and heated to 60 °C for half an hour. At the same temperature, the solution was reacted with the dropwise addition of 8 mL methacrylic anhydride (Sigma-Aldrich) and stirred. After 3 hours, the reaction was stopped by adding 300 mL DPBS to dilute the solution and dialyzed in dialysis tubes immersed in deionized water for 7 days. After dialysis the contents are transferred into Falcon tubes and stored at -80 °C for at least 2 hours. Lyophilization of these tubes for 5 days yields GelMA, appearing as a fibrous white foam.

ELP synthesis

An E. coli strain inserted with a plasmid engineered to grant kanamycin resistance and encoded for ELP production was taken from -80 °C storage and inoculated in 10 mL of Luria-Bertani (LB)

Broth containing kanamycin (50 μg/mL). This starter culture was matured overnight in a shaker incubator held at 37 °C and 300 rpm. The culture was then transferred into 1.5 L batches of Terrific Broth also containing kanamycin (50 μg/mL) and returned to the shaker incubator for 30 hours. The batches were afterwards centrifuged at room temperature, 17000xg for 20 minutes. The precipitate was collected and resuspended in lysis buffer (5.84 g-NaCl/L, 0.48 g-$MgCl_2$/L, 1.00 mL-βMe/L in (1x) TE Buffer) and kept overnight at 4 °C. The next day, the mixture was sonicated by a probe for 15 minutes and returned to 4 °C overnight. For the next four days, inverse transition cycling was applied with one cycle of cold and warm spin per day (conducted at 17000xg for 30 minutes). On the fifth day, one final cold spin occurs, after which the solution is transferred to dialysis membranes and dialyzed with milli-Q water (changed once per day) at 4 °C for 7 days. The purified solution was frozen at -80 °C for at least 2 hours and then lyophilized for 5 days to yield ELP.

Methacrylated Elastin-like Polypeptide (mELP) synthesis

ELP was dissolved in 4 °C milli-Q water (10% w/v), stirring while in an ice bath in the fridge. Methacrylic anhydride was added dropwise at a ratio 0.15*the volume of the milli-Q solution. The mixture was stirred continuously in the ice bath for 16 hours, to then be diluted with 4x volume of cold PBS. This solution was transferred to dialysis cassettes for 4 days, dialyzed against milli-Q water (changed once per day). These contents were then frozen at -80 °C for at least 2 hours and lyophilized for 5 days to yield mELP.

^{1}H Nuclear Magnetic Resonance (NMR) Analysis

The degree of methacryloyl functionalization of polymers such as GelMA have a well-established method of study, primarily through quantifying the signals of free lysine ^{1}H-NMR groups with increased degree of methacrylation [46, 47]. Providing a comparison for the area under these respective peaks within a crosslinked sample versus an uncrosslinked prepolymer solution was used to quantify the degree of crosslinking. ~10 μg samples of both bioink layers (GelMA and 1:1 mELP/GelMA) were thus taken in crosslinked and uncrosslinked states and dissolved in 1 mL dimethyl sulfoxide (DMSO-d_6) in 37 °C, before being prepared for study with proton nuclear resonance (^{1}HNMR). Performed using a 400 mHz Bruker AV400 spectrometer.

Bioink Preparation

Both the inner layer (10% (w/v) GelMA) and outer layer (7.5% (w/v) mELP:7.5% (w/v) GelMA) were dissolved in DPBS containing 1.9% (w/v) TEA , 1.2% (w/v) VC, and 1mM Eosin Y. Contained in an aluminum-wrapped Falcon tube, the inner layer ink was placed in a 37 °C incubator for 1 hour. Considering mELP's greater solubility at lower temperatures, the outer layer ink was placed in ice bath at 4 °C for 1 hour.

Carbopol Support Bath Preparation

450 mg of Carbopol ETD ('Easy-to-disperse') polymer is dissolved in 25 mL of DPBS and vortexed until fully immersed. Afterwards, 1 mL of 10 M NaOH was added to the solution in 2 equal parts (500 μL *2). This solution was centrifuged at 5,000 rpm for 10 minutes, and then vortexed until the gelated medium was uniform throughout. The Carbopol support bath was then stored at 4 °C.

Mechanical Properties

The solutions of each respective ink were pipetted into polydimethylsiloxane (PDMS) molds of rectangular geometry (12 x 4.5 x 1 mm) for tensile testing and of cylindrical geometry (5 mm diameter, 3 mm height) for cyclic compression testing. To allow sufficient time for coacervation to occur, the samples were left at room temperature for 15 minutes prior to crosslinking. Tensile and Compression tests were both conducted with an Instron 5542 Universal machine and recorded through the Bluehill Universal software.

Tensile Test: Both ends of the rectangular hydrogel samples were adhered upon transparent, double sided, adhesive polyethylene terephthalate (PET) sheets and loaded onto the Instron with the tensile claws configured. The hydrogels were then stretched by the tensile grips at a speed of 1 mm/min, continuing until the material ruptured. The tensile stress (kPa) and strain (mm) were collected from the device and then utilized to calculate the ultimate stress, ultimate strain, and the Young's Modulus. Both ultimate stress and strain were gathered from the recorded measurements at the point of fracture, and the modulus was retrieved by determining the slope of the linear stress-strain plot at 10% strain level.

Cyclic Compression Test: The cylindrical shaped samples for each material were loaded onto the Instron in its compression plate configuration. After loading, the plates were manually brought down until the sample was held between with no deformation or squishing. The samples were then compressed and decompressed in cycles of 5 for maximums of 10% strain, 20% strain, and so on until 50%. Each compression/decompression ran at a speed of 5 mm/min, regardless of the maximum strain for the cycle. The compressive stress (kPa) and strain (mm) were collected from

the device's recordings and then utilized to calculate the compressive modulus and the energy loss at the fifth cycle. The compressive modulus was determined from the slope of the initial linear region of the first cycle, while the energy loss was calculated as the difference between the stress-strain integrals of the compression and decompression curves at cycle five.

Swelling Test: Cylindrical samples were retrieved, lyophilized, and weighed for the inner and outer layer materials, as well as a few other materials for reference. Recording this weight as the 0 h, the samples were immersed in DPBS in a 24-well plate separately. The samples were lyophilized again and re-weighed at 2, 4, 8, 10, 12, 24, 72 hours to determine the change in dry mass after swelling.

The swelling percent was thus calculated by,

$$swelling\%_{1-0} = \frac{W_1 - W_0}{W_0} * 100\%$$

where W_1 is the weight of polymer at t = 1 and W_0 is the weight of the polymer at t = 0.

Degradation Test: Cylindrical samples were retrieved, lyophilized and weighed for the inner and outer materials, as well as a few other materials for reference. Recording this weight as day 0, samples were immersed in 20 µg/mL-PBS collagenase type II (ThermoFisher, 305 U/mL) solution. The samples were lyophilized again and re-weighed at 1, 2, 3, 5, 7, 14 day intervals to determine the change in dry mass after degradation.

The degradation percent was calculated by,

$$degradation\%_{1-0} = \frac{W_0 - W_1}{W_0} * 100\%$$

where W_1 is the weight of polymer at t = 1 and W_0 is the weight of the polymer at t = 0.

Bioprinter Operation

We used an Allevi 3 bioprinter, a 3-nozzle direct bioprinter with individual systemic control for each printhead. The bioprinter was operated via the proprietor's designated software, to be found at bioprint.allevi3d.com. The program granted instantaneous alteration to the printing speed, extrusion pressure, and temperature of the respective printhead, as well to load a .stl file for printing. When printing, the bioprinter interpreted and recreated the .stl image into the Carbopol support bath. When printing both the inner and outer layers of the construct, each layer was printed in series. Optimization of printing conditions were determined according to the variation in performance with respect to printing speed, extrusion pressure, and temperature. Printed constructs were carefully extracted from the bath using a spatula and then washed gently with DPBS to remove any excess Carbopol.

Statistical Analysis

Statistical analyses were conducted using unpaired, one-tailed Welch's t-test for single comparison sets with a 95% confidence interval. Multiple comparisons were made using ordinary one-way ANOVA tests with a 95% confidence interval. A minimum of n = 3 samples were used for each test.

CHAPTER 3: Results and Discussion

Analysis of the ^{1}HNMR analysis for both hydrogel systems revealed the presence of the methacrylate and methacrylamide peaks around 5.3 and 5.7 parts per million (ppm), respectively (labeled α and in Figure 4 C, E). As the H protons reside on opposing ends of a double bond, they are constrained to separate electronegative environments due to the proximity of the methacrylate and methacrylamide regions. Splitting of the ^{1}HNMR peaks were thus expected and expressed to a slight degree in uncrosslinked samples. When compared with ^{1}NMR spectra of crosslinked samples, these peaks are greatly reduced in magnitude, evidencing the successful linkages which have been made. This is consistent with previous findings concerning GelMA and ELP [52]. The degree of crosslinking was determined to be ~55% for the 10% (w/v) GelMA bioink, and ~68% for the 7.5% mELP/ 7.5% GelMA (w/v) bioink.

During the development of the mELP/GelMA hydrogel, it was observed that the fibrous foam of mELP was dissolved in water when kept at low temperature ranges around 4 °C. GelMA meanwhile has a variable solubility at that temperature, altering primarily on which animal the gelatin had been sourced from. Porcine GelMA remains insoluble in DPBS at 4 °C, while fish GelMA can readily dissolve. Therefore, all mELP/GelMA hydrogel mixtures were concocted using fish GelMA, while ink layers without mELP employed porcine-sourced gelatin.

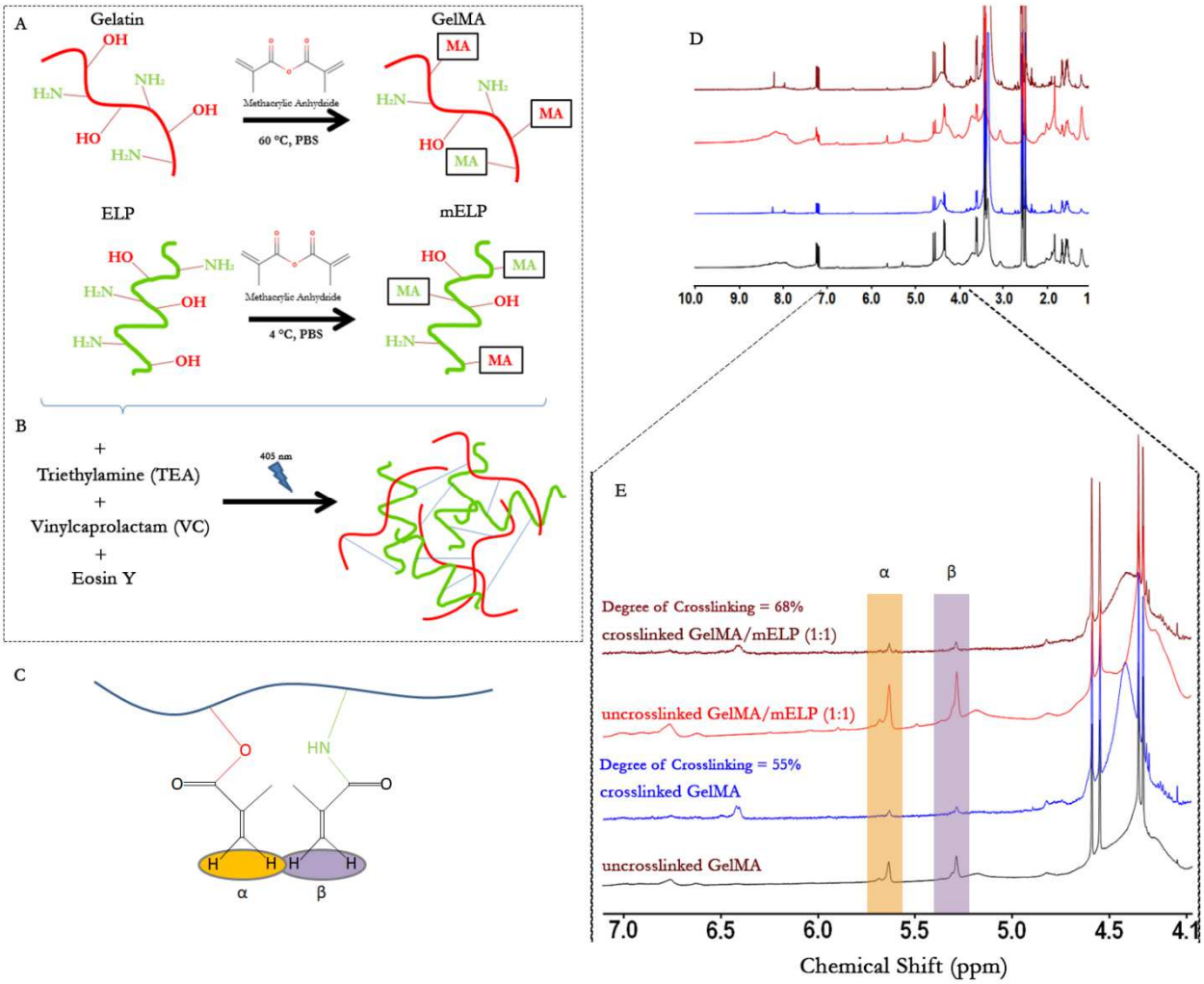

Figure 4. Chemical characterization of gelatin methacryloyl (GelMA) and methacrylated elastin-like polypeptide (mELP). (A) Methacrylation of gelatin and ELP producing functionalized methacryloyl and methacrylamide groups through respective reactions with methacrylic anhydride. (B) A mixture of GelMA and ELP prepolymer was dissolved in a solution containing an Eosin-Y based photoinitiator and the solution was exposed to visible light (405 nm) to form a composite hydrogel through the formation of covalent linkages between methacryloyl functional groups. (C) Methacryloyl and methacrylamide groups and their characteristic protons (labeled α and β respectively), which were removed during the covalent linkage formation of

photocrosslinking. (D-E) HNMR spectra of uncrosslinked GelMA, crosslinked GelMA, uncrosslinked GelMA/mELP (1:1), and crosslinked GelMA/mELP (1:1) (bottom→top). The acrylate peaks highlighted reveal the degree of crosslinking via the difference in peak intensity.

One of the initial steps taken towards determining the polymer composition of the bioink was to study the effect of hydrogel compositions and ELP methacrylation on the mechanical properties of the resulting hydrogel. As shown in Figure 5, at a fixed final polymer concentration of 15%, it was found that the methylation of ELP improved the mechanical properties of the resulting composite hydrogel. For example, the ultimate stress of GelMA/mELP was 29.26 ± 5.97 kPa, which was significantly higher than GelMA/ELP hydrogel (10.14 ± 3.43 kPa) (Figure 5A). In addition, the strain was significantly higher in GelMA/mELP ($35.14 \pm 8.45\%$) than GelMA/ELP ($21.76 \pm 2.80\%$) (Figure 5B). A similar trend was observed for the elastic modulus which was 135.1 ± 24.24 kPa for mELP/GelMA and 59.80 ± 7.72 kPa for ELP/GelMA (Figure 5C). As previously described, the utility of ELP is intended to enhance stretchability to better mimic the native urethra, and methacrylated ELP achieves this most successfully in the hydrogel blend with GelMA. Independently, ELP has previously been characterized to possess remarkable stretchability ($395 \pm 10\%$ for 15% (w/v) ELP) [55]. However, creating mixed polymer gels of ELP and GelMA receive much reduce strain character, consistent with the findings shown below [56]. Without linkage formation from methacryloyl and methacrylamide groups, ELP provides less structural support in a GelMA blend. With this data we decided that methacrylating ELP to make mELP provided the greatest mechanical viability for the construct.

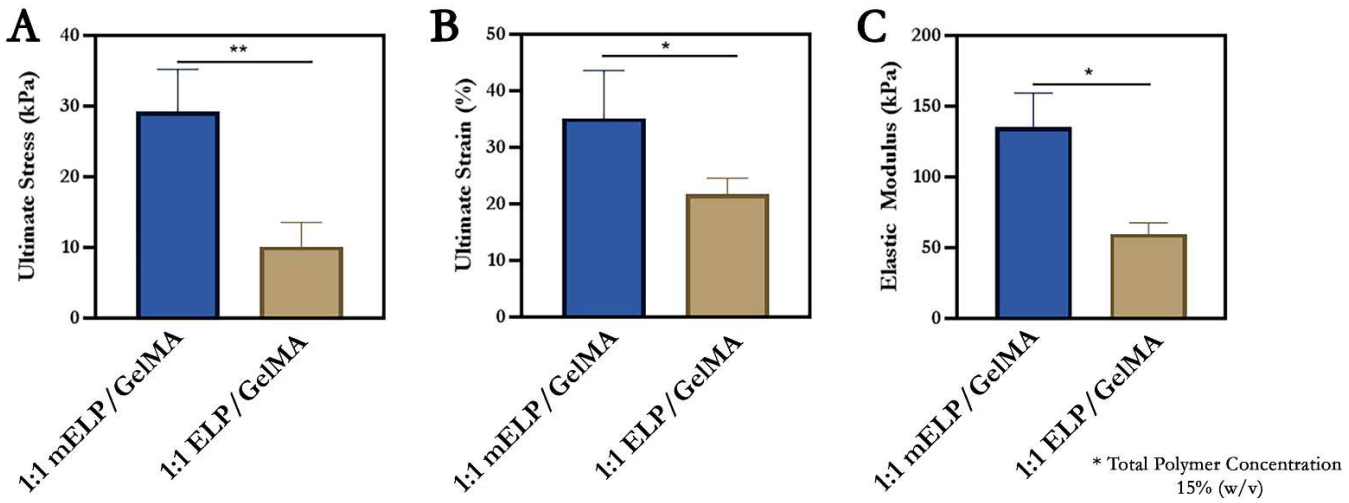

Figure 5. Effect of ELP methacrylation. Tensile ultimate stress (kPa), ultimate strain (%), and elastic modulus (kPa) for 15% total polymer concentration (w/v) samples of 1:1 mELP/GelMA and 1:1 ELP GelMA. (* $p < 0.05$, ** $p < 0.01$)

Next, we studied the effect of final polymer concentrations and different ratios of GelMA/mELP on the properties of the resulting hydrogel including tensile strength, strain, elastic modulus, compressive modulus, and energy loss. Swelling and degradation profiles were also compared. The final polymer concentrations were 10% and 15%. This decision was selected to maintain similar hydrogel specifications as previous studies [48], as well as to ensure no cytotoxic effects. It has previously been observed that GelMA based biomaterials exhibit regional cytotoxicity above 25% (w/v), and our preliminary testing had determined that hydrogels with 5% (w/v) final polymer concentration were difficult to handle and would often fragment. Previous studies utilizing a blend of GelMA and methacrylated tropoelastin (MeTro) maintained an overall weight percentage of 15% with success, and thus was selected for our studies here [48]. Interest in a lower percentage hydrogel (i.e., 10% GelMA) for the inner layer of the biomaterial scaffold was kept promoting more rapid cellular adhesion and proliferation and provide an improved rate of

healing while the external layer with 15% concentration could maintain the scaffold's structural support.

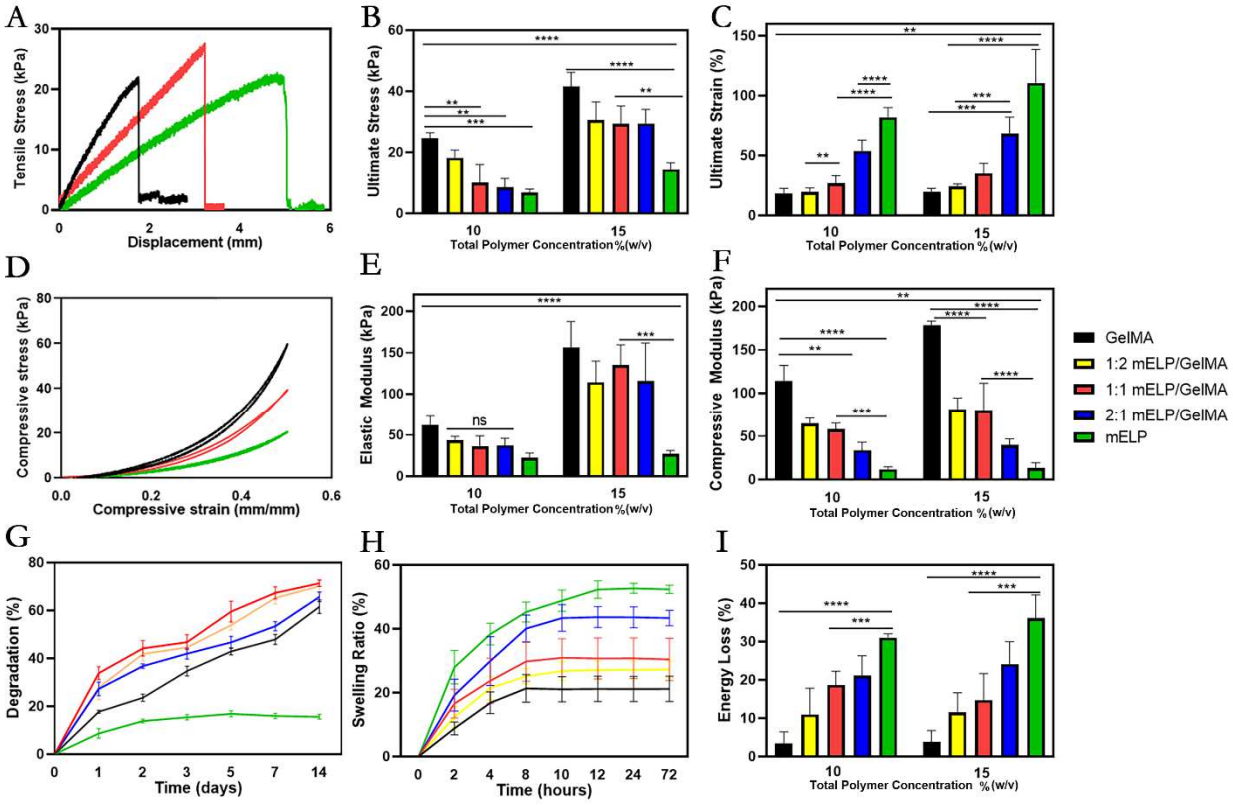

Figure 6. Mechanical characterization, swelling, and degradation of gelatin methacryloyl (GelMA)/methacrylated elastin-like polypeptide (mELP) hydrogels. (A) Characteristic tensile curves. (B) Ultimate stress. (C) Ultimate tensile strain. (D) Characteristic cyclic compression curves upon the fifth cycle. (E) Elastic modulus. (F) Compressive modulus. (G) Degradation profile. (H) Swelling ratio profile. (I) Energy loss calculation. (* $p < 0.05$, ** $p < 0.01$, *** $p < 0.001$, and **** $p < 0.0001$)

Tensile testing yielded results which were expected for the sample sets tested, as every hydrogel with the greater overall weight percent (15% w/v) achieved higher ultimate stress and strain than hydrogels with a lower percentage (10% w/v) (Figure 6 B,C). This is justified through

the greater number of covalent linkages present as a higher concentration of polymers propagates the length of the sample. At 15% overall weight percent, the ultimate stress for GelMA (41.70 ± 4.4 kPa) far exceeds mELP (14.42 ± 2.13 kPa), evidencing GelMA's tensile resilience (Figure 6B). mELP expectedly had much greater ultimate strain than GelMA (110.54 ± 28.07% versus 19.48 ± 3.17%, respectively) (Figure 6C). Blended hydrogels observably performed at ranges in-between each pure material, an observation which remains consistent throughout the mechanical characterization. Increasing mELP proportions in the bioink generally saw a drop-off in the elastic modulus, ranging from 156.03 ± 31.47 kPa for GelMA down to 26.77 ± 4.16 kPa for mELP (15% w/v) (Figure 6E). The elastic modulus was relatively high for equal blends of mELP/GelMA (1:1) (135.1 ± 24.24 kPa), duly encouraging its selection as the primary bioink in printing the durable outer layer to the tubular construct.

Compressive testing yielded similar results for the compressive modulus with a steady drop-off as proportions of mELP produced, with a high 15% GelMA (177.93 ± 4.96 kPa) down to 15% mELP (13.31 ± 6.11 kPa). (Figure 6 F). Energy loss calculations however revealed a trend in the opposite direction, with the loss rising from 3.82 ± 2.96% in GelMA to 36.07 ± 6.10% in mELP after five cycles of compression (Figure 6I). An explanation for this greater energy loss with mELP could be found in the coiling geometries that mELP tends to inhabit; while the greater extensibility is observed as a result of this composition, it is likely that once perturbed much of the potential held in these polypeptide coils is expended, and subsequent compression of mELP cannot match its initial resilience.

Pure mELP had predictably the lowest degradation profile over the fourteen-day period of immersion in the type II collagenase solution, which is due to the fact that ELP primarily degrades more significantly with elastase enzyme rather than collagenase (which degrades GelMA hydrogel

chemistry) (Figure 6 G). However, the mixed-solution polymer samples degraded more than the pure GelMA despite mELP presence. This is explained by the proportionally lighter GelMA presence in these samples while the kinetics of enzymatic degradation would be unchanged. The swelling tests revealed a gradient of a dropping swelling ratio following the increase of GelMA in hydrogel samples, an expected trend as it matches previous findings [49]. Swelling ratio decreases as the overall weight percentage of GelMA rises as the porous channels between the polymer linkages grow tighter and less accommodating to H_2O storage.

Mechanical characteristics provided us with the justification to select an equally mixed ratio of mELP/GelMA (1:1), as with this material ratio we can achieve a bridging of GelMA's high moduli and ultimate tensile strength while also awarding increased stretchability from mELP. Utilizing this ratio at 15% w/v overall provides us with a versatile bioink to utilize on the outer layer of the bioprinted scaffold, capable of supporting the inner layer as cells proliferate. Previous work characterizing a polymer blend of mELP/GelMA for a sealant-patch application observed a physical characterization similar to that shown in Figure 6 [52]. The affected trends in performance as the mELP/GelMA ratio were similarly observed. For example, increased proportions of GelMA were also seen to improve both the elastic and compressive moduli, while extensibility significantly rises as mELP proportion rose. However, the order of magnitude for tensile and compressive mechanics are notably dissimilar between this work and Unal *et al.*, which can be attributed to the difference in total polymer concentration. As their application was intended for a sealant-patch use, selecting a 30% (w/v) total polymer concentration provides improved mechanical support and reduced swelling. However, polymer concentrations that high may reduce cellular proliferation, potentially due to the constrained interstitial space within the gel as well as changes in cytotoxicity.

Utilizing the same 15% (w/v) total polymer concentration as this work, Lee *et al.* generated a similar set of mechanical characteristics for a 1:1 blend of GelMA with another elastin-based polymer for bioprinting vasculature, methacrylated tropoelastin (MeTro) [48]. Trends observed for the 15% (w/v) MeTro/GelMA polymer system are markedly similar to 15% (w/v) mELP/GelMA; pure GelMA attains the greatest elastic and compressive moduli but sustains the greatest energy loss and is least extensible. For mechanics, the ultimate stress of MeTro/GelMA (47.9 ± 2.6 kPa) is a similar order of magnitude to mELP/GelMA (29.3 ± 6.0 kPa). Comparing strain, these materials are quite close in behavior (33.1 ± 8.3% and 35.1 ± 8.5%, respectively). However, the compressive modulus of mELP/GelMA exceed what was reported for MeTro/GelMA (80.2 ± 31.2 kPa and 49.2 ± 8.7 kPa, respectively. Annabi *et al*. also report mechanics for MeTro/GelMA, corroborating many mechanical properties for comparison with mELP/GelMA [57]. For example, they report for 1:1 MeTro/GelMA extensibility of 20.4 ± 1.9% and ultimate stress 15.6 ± 4.6 kPa. The fluctuation between these two sources for the mechanics of MeTro/GelMA are notable, but for comparative purposes with mELP/GelMA they affirm a similar magnitude of properties between MeTro and mELP when forming polymer blends with GelMA.While in both cases the polymer blend appears to provide mechanical performance in-between the pristine samples, the unique geometrical and chemical differences between mELP & GelMA result in varied performance between the two. It would appear from Lee *et al.* that highly coiled geometry of MeTro may encourage little energy losses, though the compression of mELP requires a greater input of force.

A relevant observation worth noting is the increased handling difficulty as the presence of mELP in the sample material increased. These observations ranged from an increased length of time required to observe true dissolution of the polymer into the crosslinking solution to increased

viscosity & resistance to pipetting. In order to accommodate these issues, a longer window of time was given for mELP carrying solutions to dissolve & homogenize, and pipette tips were cut to increase the cross-sectional area from which the fluid could flow.

Another significant observation during the collection of mechanical data was the variation in performance that was observed in hydrogels composing a mixture of GelMA and mELP when left for a half-hour period at room temperature before crosslinking and testing. mELP/GelMA bioinks which were immediately crosslinked had significantly lower performance than those which were given this time at room temperature, yielding an ultimate stress of 18.65 ± 2.84 kPa when immediately crosslinked versus 31.07 ± 5.81 kPa when given 0.5 hours at room temperature (Figure 7A). Ultimate strain also improved when the prepolymer solution was given this time (39.16 ± 7.51%) than to be directly crosslinked (39.16 ± 7.51%) (Figure 7B). The elastic modulus nearly doubled (129.65 ± 17.00 kPa) compared to its performance without this time (59.33 ± 9.94 kPa) (Figure 7C). This is due to a process known as coacervation, whereby GelMA and mELP spontaneously aggregate towards themselves respectively in a liquid-liquid separation of an initially homogeneous solution. Initially held at 4 °C for mELP to dissolve into the solution, the difference in charge & hydrophilicity between the polymers means that as the temperature warms over time prior to crosslinking the polymers will orient themselves. While spontaneous at low temperatures, this coacervation behavior is significantly more impactful at room temperature. Samples crosslinked after requisite time at room temperature we postulate are more likely to form linkages amongst like polymers rather than between unlike polymers, which would explain the change in performance. While coacervation affects all polymer samples, our results suggest this effect is not nearly as impactful for the pure GelMA bioink, as no statistical significance emerged for this set (Figure 7A-C). A plausible conclusion to draw is that coacervation more considerably

improves mixed-polymer gels like mELP/GelMA than unary gels like pure GelMA. As aggregation improved the performance of mixed-polymer solutions, we conducted all mechanical analysis after the material has had half an hour to coacervate at room temperature after dissolving.

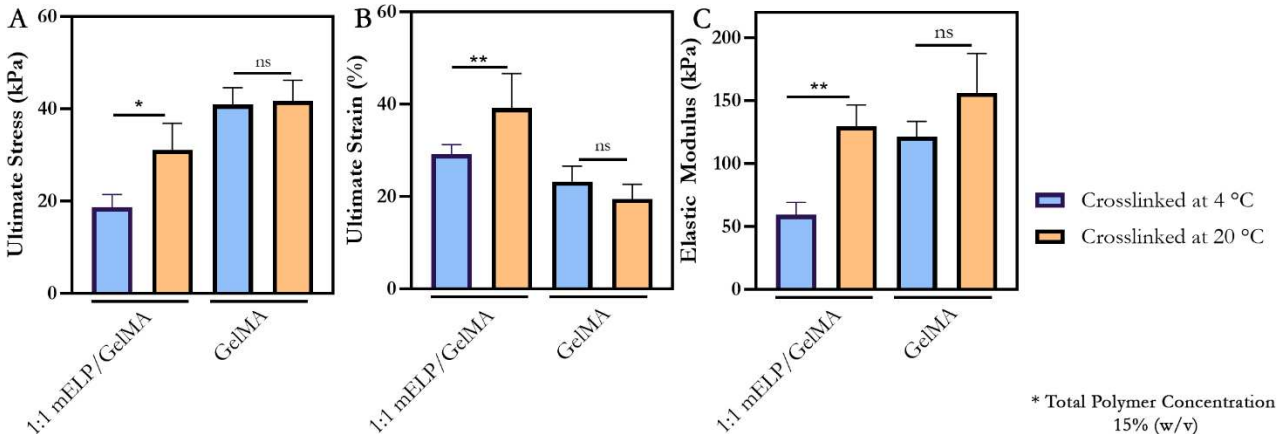

Figure 7. Mechanical impact of coacervation. Tensile ultimate stress in kPa (A), ultimate strain % (B), and elastic modulus in kPa (C) for 15% (w/v) total polymer concentrations of selected bioinks. (* $p < 0.05$, ** $p < 0.01$)

The Allevi 3 3D-bioprinter is a direct bioprinter, and extruded loaded ink through a syringe with the supply of pneumatic pressure (Figure 8A). The bioprinting optimization underwent many stages to test the three relevant variables tunable by the Allevi 3 3D-bioprinter: printing speed (mm/s), extrusion pressure, and temperature (°C) (Figure 8B). A needle gauge of 23 (0.337mm inner diameter) selected for extrusion for both inks to control the cross-sectional area of ink flow during pneumatic-induced fluid flow. For each set of conditions, multiple prints were produced to qualitatively determine the best adherence of the printed product to the dimensions set in the .stl file. Bleeding, inconsistent fluid flow, or other issues are thus observed with respect to the deviation in the printed image, which were then categorized according their resolution. Printed samples were considered 'poor' if there was excessive bleeding or substantially little printing, while 'good' conditions were specified if the printed product maintained uniform shape &

consistent dimensions. As Figure 8C enumerates, the printing optimization for each bioink yielded for temperature 30 and 8 °C, printing speed of 8 mm/s and 5 mm/s, and extrusion pressure 4 psi and 15 psi for the 10% (w/v) GelMA bioink and 15% (w/v) 1:1 mELP/GelMA bioink, respectively. The optimized conditions selected for each respective layer vary significantly, primarily due to mELP's sensitivity towards temperature in the blended bioink layer. Separate thermal control for each ink layer is a necessity for the design of this direct bioprinter, as the 10% GelMA layer can easily print at 30 °C which would be impossible for 15% 1:1 mELP/GelMA.

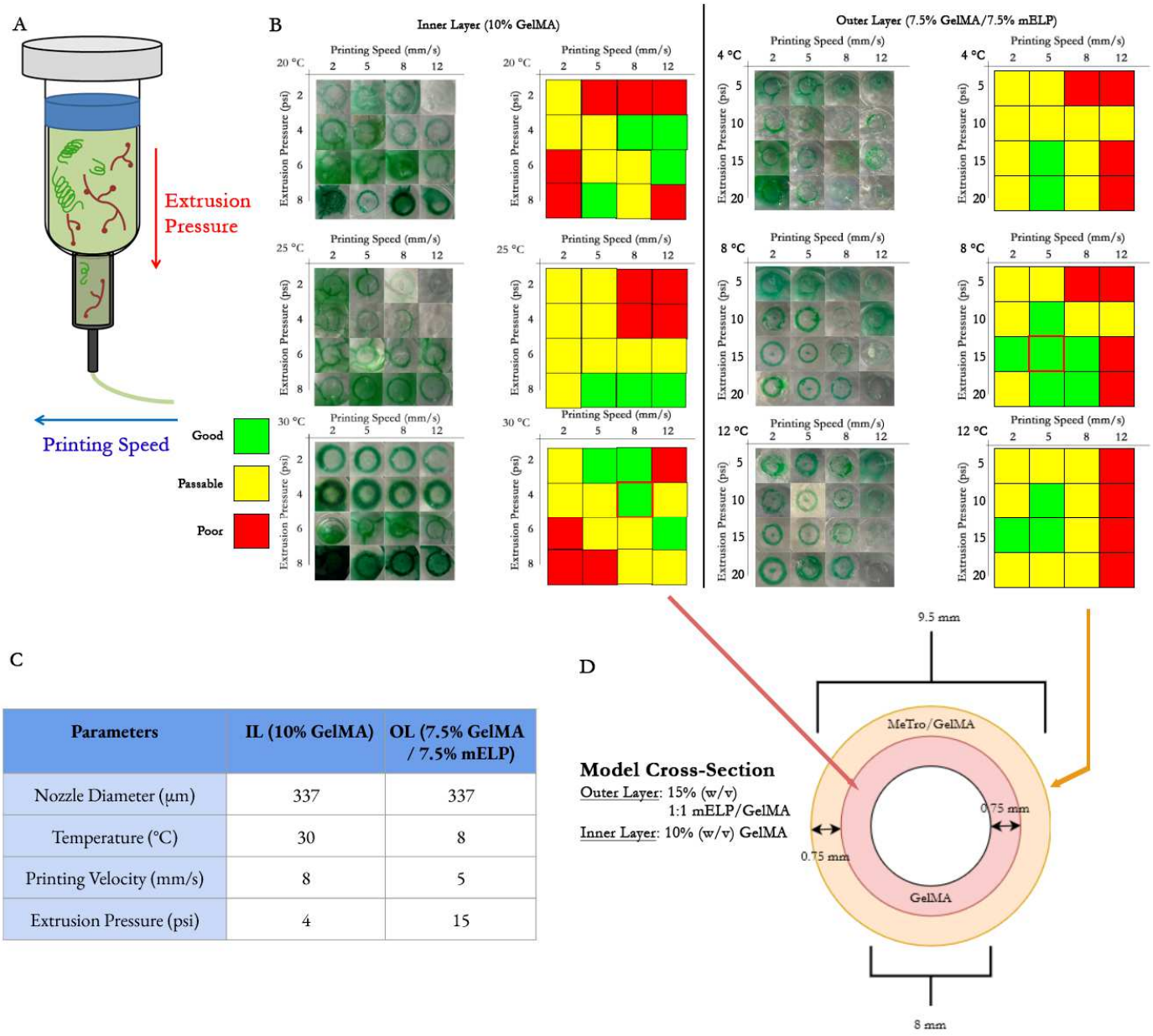

Parameters	IL (10% GelMA)	OL (7.5% GelMA / 7.5% mELP)
Nozzle Diameter (μm)	337	337
Temperature (°C)	30	8
Printing Velocity (mm/s)	8	5
Extrusion Pressure (psi)	4	15

Figure 8. Bioprinting optimization and bioink treatment. (A) Schematic representation of bioprinting with variable printing speed and extrusion pressure (B) Printing optimization of 10% (w/v) GelMA (left) and 15% (w/v) 1:1 mELP/GelMA (right) bioinks with respect to printing speed (mm/s), extrusion pressure (psi), and temperature (°C). (C) Optimized printing parameters for

inner layer (IL) and outer layer (OL). (D) Schematic cross-sectional view of two-layered urethral construct with 8mm diameter IL and 8.75 diameter OL, each with thickness 0.75mm.

Comparing the printing parameter optimization between 15% (w/v) 1:1 mELP/GelMA and that of 15% (w/v) 1:1 MeTro/GelMA in the report by Lee *et al*., it can immediately be seen that optimal printing temperatures between both polymers are similar at 8 °C [48]. However, the printing speed and extrusion pressure utilized for optimized MeTro/GelMA is much greater than for mELP/GelMA. Reasons behind this increased stress required to induce optimal MeTro/GelMA printing include the utility of sacrificial gelatin embedded in their bioink, intended to shield cells in the bioink from intense shear stresses. The use of this additional material thickens their bioink and would reasonably necessitate greater induced forces and velocities to induce fluid flow. It is worth additionally noting that while in this work an Allevi 3 printer was employed, their work utilized an INKREDIBLE+ Cellink printer, and variation commonly emerges between brands and instrumentation.

For the dimensional design of the bioprinted construct, we determined an interior diameter of 8mm and an exterior diameter of 9.5mm**;** each respective layer is thus 0.75mm thick each (Figure 8 D). These sizes were intended to be consistent with the dilated radius of native male rabbit urethra (NZ) during urine flow, to ensure the scaffold doesn't act as a stricture site due to pressure funneling [15, 51]. These dimensional specifications ensure that the printed product can easily be utilized during any subcutaneous implantation experiments later in the project's development or testing the model's efficacy *in situ*.

After extrusion into the Carbopol ETD bath, extractions were attempted by removing the construct from the well with a spatula and then rinsing with warm PBS to remove excess bath gel

(Figure 9). We observed difficulty completely separating the printed construct at its small size from Carbopol material, particularly within the lumenar cavity in the center of the cylinder. Propriety sources in Lubrizol utilizing Carbopol baths recommended using low concentration solutions of bases such as calcium chloride ($CaCl_2$) as a wash instead of PBS to neutralize the bath gel [50]. However, when attempted with 0.11 M $CaCl_2$ the gel broke into opaque, sticky white flakes which adhered to the printed product, and was ultimately deemed undesirable for our purposes. Successful extraction was however achieved using the warm PBS wash with gentle agitation for each printed layer independently; the printing of both layers simultaneously to form the full urethral construct remains work for the future direction of the project (see that section for more detail).

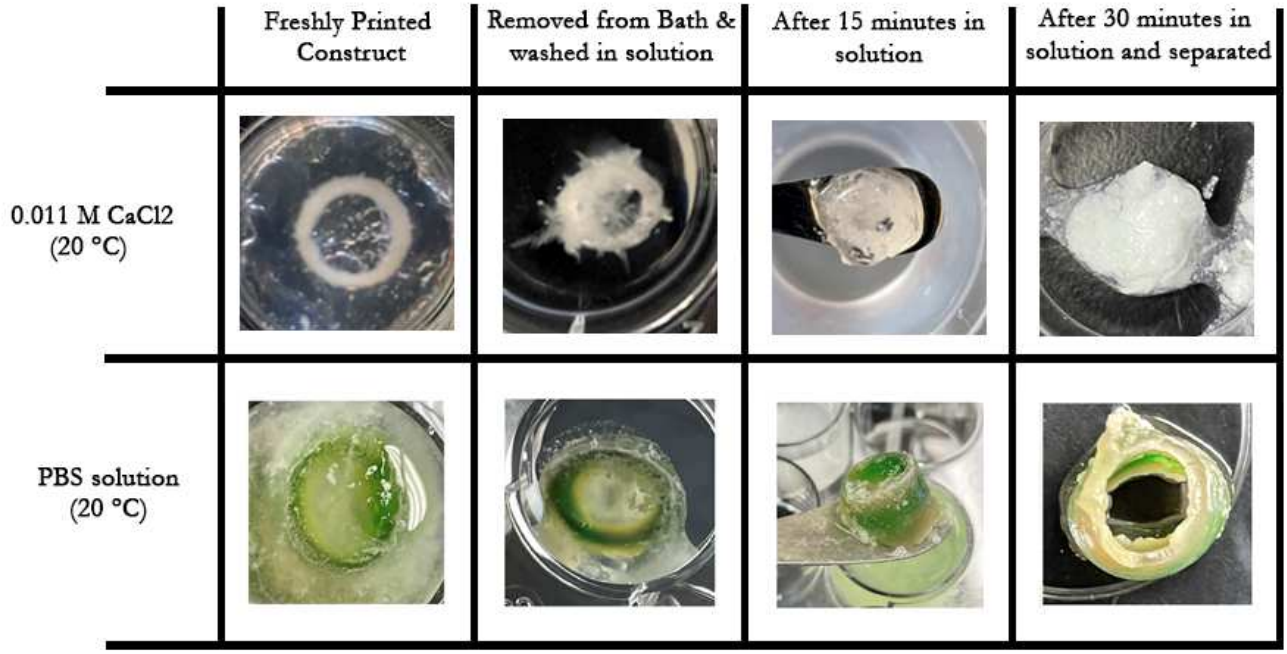

Figure 9. Carbopol Gel Extraction. Method of executing a Carbopol ETD bath extraction using 0.011 M CaCl2 and PBS.

CHAPTER 4. Future Directions and Conclusion

This thesis reviews the niche surrounding urological grafts, their conventional use, and opportunities for advancement. We introduced 3D-bioprinting as a promising alternative method for scaffold fabrication and eliminate the need for a donor site, and how the various methods of printing compliment the process or possess opportunities for innovation. Then, we took cursory looks at other biomaterial fabrication methods in electrospinning and molding to better learn how 3D-bioprinting stands as a method of urethral scaffold production on a macroscopic level. This literature review (which has been compiled and written for the intent of a published review article) provided the team with the technical knowledge & expertise to design our own hydrogel system for urethral reconstruction. Use of mELP and GelMA is novel for urethral bioprinting is novel within this niche, and utilizes well-characterized, reliable, and commercially available chemistries in an exciting direction for this emerging field. The chemical characterization of the hydrogel formation and quantification of the system's mechanical limitations brought us clarity with regard to the system's design, and the non-Newtonian flow of each respective bioink layer has been optimized for a high fidelity in printed constructs.

The work presented in this thesis represents the beginning of a sizeable project, and many experiments remain to develop the utility of 3D-bioprinting towards the fabrication of urethral scaffolds using mELP and GelMA. Briefly we will here enumerate the subsequent steps that would pave forward the development of this project. Firstly, printing and extracting a two-layer cylindrical construct with our hydrogel system would provide useful visual images to show the method used in synthesis. Using the Allevi 3 bioprinter, we have access to multiple printheads, but each layer must be printed sequentially in a direct-extrusion manner. Both the 10% w/v GelMA bioink and the 15% w/v 1:1 mELP/GelMA bionk have vastly different optimized printing

parameters, and so while both printheads require tuned calibration, each must have a carefully maintained temperature, pressure, and printing speed.

Prior to incorporating cells directly into the ink, a proof-of-concept seeding using relevant urethral cell lines would be very beneficial to the project. Such an experiment could be achieved using a 2D-dropwise seeding technique and would provide us the opportunity to gain useful *in vitro* data as to the cytocompatibility and cellular proliferation of the construct (using Prestoblue and Live/Dead culture assays. Urothelial cells (ATCC PCS-420-010: Primary Bladder Epthelial Cells (A/T/N); Normal, Human (BdEC)) and smooth muscle cells (ATCC PCS-420-012: Primary Bladder Smooth Muscle Cells; Normal, Human (HBdSMC)) would be the primary cell lines for our experiments, though work will likely first be conducted with fibroblasts (ATCC 201-012: Primary Dermal Fibroblast; Normal, Human, Adult (HDFa)) as they are easiest to culture and assist us with inevitable troubleshooting.

Subsequent *in vitro* testing would incorporate a dense population of these cell lines into the bioink prior to printing and running the printing experiment and extraction all under sterile conditions. It may serve to separate the cells incorporated with the respective layers in which the model would predicate them to appear (urothelial cells in the inner ring, smooth muscle in the outer ring), but it might also provide interesting results to observe what emerges if equal proportions of both cell lines are present in both bioinks. Urothelial cells and SMCs naturally aggregate like towards like, and observing differences that may emerge in the grain of scaffold tissue may help determine the optimal means of bioprinting such constructs. For these experiments, it is vital that we determine the seeding density for each line, as well as endpoints and outcomes. The pressurized extrusion of ink is a process which will certainly be strenuous for any cells embedded into the ink, and the cell density when printing will need be very high. Imaging these

samples will also present some challenge as the printed structure is of course three-dimensional, and so it might be determined that a cross section of a sample that has been printed and cultured will be taken to observe cellular behavior. Even further, subcutaneous implantation or experiments *in situ* would provide even greater characterization of the mELP/GelMA scaffolds' feasibility in surgical use, as the scaffold would inhabit conditions as close as possible to those necessitated for use in urethral reconstruction or urethroplasty.

Bibliography

1. Hull, C. W. Apparatus for production of three-dimensional objects by stereolithography. US Patent 4575330 (1986).
2. O'Brien KW, Xu PA, Levine DJ, *et al.*, 2018, Elastomeric Passive Transmission for Autonomous Force-Velocity Adaption Applied to 3D-Printed Prosthetics. *Sci Robot.*, 3: eaau5543. https://doi.org/10.1126/scirobotics.aau5543
3. Ho CM, Ng SH, Yoon YJ, 2015, A Review on 3D Printed Bio-Implants. *Int J Precis Eng Manuf,* 16:1035-46
4. Whulanza Y, Hidayaturrahmi P, Kurniawati T, et al., 2017, Realization and Testing of Multi-Material 3D Printer for Bone Scaffold Fabrication, Depok City, Indonesia, p. 040001. https://doi.org/10.1063/1.4976786
5. Abuzairi T, Sumantri NI, Irfan A, et al., 2021, Infrared Thermometer on the Wall (iThermowall): An Open Source and 3-D Print Infrared Thermometer for Fever Screening. HardwareX, 9:e00168. https://doi.org/10.1016/j.ohx.2020.e00168
6. Norman J, Madurawe RD, Moore CM, et al., 2017, A New Chapter in Pharmaceutical Manufacturing: 3D-Printed Drug Products. Adv Drug Deliv Rev, 108:39-50 https://doi.org/10.1016/j.addr.2016.03.001
7. Kang H.-W, Lee SJ, Ko IK, Kengla C, Yoo JJ, Atala A, A 3D bioprinting system to produce human-scale tissue constructs with structural integrity. *Nat. Biotechnol.* 2016, 34, 312-319
8. Shafiee A, Atala A (March 2016). "Printing Technologies for Medical Applications". Trends in Molecular Medicine. 22 (3): 254–265. doi:10.1016/j.molmed.2016.01.003. PMID 26856235

9. Charsoula Anna, et al. "Imaging of the normal male urethra from the neonate to the elder: radiologic anatomy in fluoroscopic urethrography." European Congress of Radiology-ECR 2014, 2014
10. Patel, D. B., Luthers, C. R., Lerman, M. J., Fisher, J. P., & Jay, S. M. (2019). Enhanced extracellular vesicle production and ethanol-mediated vascularization bioactivity via a 3D-printed scaffold-perfusion bioreactor system. *Acta biomaterialia*, *95*, 236-244.
11. Zimmerman, W. Britt and Santucci, Richard A. Buccal mucosa urethroplasty for adult urethral strictures. Indian J Urol. 2011 Jul;27(3):364-70.
12. Zhang, Y. Z.; et al. Characterization of The Surface Biocompatibility of The Electrospun PCL-Collagen Nanofibers Using Fibroblasts.Biomacromolecules 2005, 6, 2583–2589
13. Ramsay, Sophie; et al. Clinical challenges in tissue-engineered urethral reconstruction. Transl Androl Urol. 2016 Apr; 5(2): 267–270.
14. Barbagli, Guido, et al. "Morbidity of oral mucosa graft harvesting from a single cheek." *European urology* 58.1 (2010): 33-41.
15. M.R. Markiewicz, J.L. DeSantis, J.E. Margarone, M.A. Pogrel, S.K. Chuang Morbidity associated with oral mucosa harvest for urological reconstruction: an overview J Oral Maxillofac Surg, 66 (2008), pp. 739-744
16. Palmer, B. W., Reiner, W., & Kropp, B. P. (2012). Proximal hypospadias repair outcomes in patients with a specific disorder of sexual development diagnosis. Advances in urology, 2012.
17. Saltzman, A. F., Carrasco, A., Colvin, A., Campbell, J. B., Vemulakonda, V. M., & Wilcox, D. (2018). Patients with disorders of sex development and proximal hypospadias are at high risk for reoperation. World journal of urology, 36(12), 2051-2058.

18. Maclean, Allan; Reid, Wendy (2011). "40". In Shaw, Robert (ed.). Gynaecology. Edinburgh New York: Churchill Livingstone/Elsevier. pp. 599–612. ISBN 978-0-7020-3120-5;
19. Zhang, K., Fu, Q., Yoo, J., Chen, X., Chandra, P., Mo, X., ... & Zhao, W. (2017). 3D bioprinting of urethra with PCL/PLCL blend and dual autologous cells in fibrin hydrogel: An in vitro evaluation of biomimetic mechanical property and cell growth environment. Acta biomaterialia, 50, 154-164.
20. L. Ouyang, C. B. Highley, W. Sun, J. A. Burdick, Adv. Mater., 2017, 29, 1604983
21. Pi Q., Maharjan S., Yan X., Liu X., Singh B., Van Genderen A.M., Robledo-Padilla F., Parra-Saldivar R., Hu N., Jia W., et al. Digitally Tunable Microfluidic Bioprinting of Multilayered Cannular Tissues. Adv. Mater. 2018;30:1706913. doi: 10.1002/adma.201706913.
22. Versteegden, Luuk R., et al. "Tubular collagen scaffolds with radial elasticity for hollow organ regeneration." Acta biomaterialia 52 (2017): 1-8.
23. Hinton, T. J., Jallerat, Q., Palchesko, R. N., Park, J. H., Grodzicki, M. S., Shue, H. J., ... & Feinberg, A. W. (2015). Three-dimensional printing of complex biological structures by freeform reversible embedding of suspended hydrogels. Science advances, 1(9), e1500758.
24. Ishii, Takuro, et al. "Deformable phantoms of the prostatic urinary tract for urodynamic investigations." Medical physics 46.7 (2019): 3034-3043.
25. Dorati, R., Colonna, C., Tomasi, C., Genta, I., Bruni, G., & Conti, B. (2014). Design of 3D scaffolds for tissue engineering testing a tough polylactide-based graft copolymer. Materials Science and Engineering: C, 34, 130-139.

26. Joshi, P. M., & Kulkarni, S. B. (2020). 3D printing of pelvic fracture urethral injuries-fusion of technology and urethroplasty. Turkish journal of urology, 46(1), 76.
27. Gudapati, H., Dey, M., & Ozbolat, I. (2016). A comprehensive review on droplet-based bioprinting: Past, present and future. Biomaterials, 102, 20-42.
28. Munaz, A., Vadivelu, R. K., John, J. S., Barton, M., Kamble, H., & Nguyen, N. T. (2016). Three-dimensional printing of biological matters. Journal of Science: Advanced Materials and Devices, 1(1), 1-17.
29. Maclean, Allan; Reid, Wendy (2011). "40". In Shaw, Robert (ed.). Gynaecology. Edinburgh New York: Churchill Livingstone/Elsevier. pp. 599–612. ISBN 978-0-7020-3120-5
30. Devillard, Raphaël; Pagès, Emeline; Correa, Manuela Medina; Kériquel, Virginie; Rémy, Murielle; Kalisky, Jérôme; Ali, Muhammad; Guillotin, Bertrand; Guillemot, Fabien (2014), "Cell Patterning by Laser-Assisted Bioprinting", Methods in Cell Biology, Elsevier, 119, pp. 159–174, doi:10.1016/b978-0-12-416742-1.00009-3, ISBN 978-0-12-416742-1, retrieved 2021-10-27
31. Malda, J., Visser, J., Melchels, F. P., Jüngst, T., Hennink, W. E., Dhert, W. J., ... & Hutmacher, D. W. (2013). 25th anniversary article: engineering hydrogels for biofabrication. Advanced materials, 25(36), 5011-5028.
32. R. Xiong, Z. Zhang, W. Chai, Y. Huang, D. B. Chrisey, Biofabrication, 2015, 7, 045011
33. Lee, V. K., Kim, D. Y., Ngo, H., Lee, Y., Seo, L., Yoo, S. S., ... & Dai, G. (2014). Creating perfused functional vascular channels using 3D bio-printing technology. Biomaterials, 35(28), 8092-8102.

34. Ziabicki, A. (1976) Fundamentals of fiber formation, John Wiley and Sons, London, ISBN 0-471-98220-2.

35. Merritt, S. R., & Exner, A. (2012). a., Lee Z, Von Recum H a.". Electrospinning and Jmaging. Advanced Engineering Materials, 14(5), B266-B278.

36. Rashid, T. U., Gorga, R. E., & Krause, W. E. (2021). Mechanical Properties of Electrospun Fibers—A Critical Review. Advanced Engineering Materials.

37. Wei, G., Li, C., Fu, Q., Xu, Y., & Li, H. (2015). Preparation of PCL/silk fibroin/collagen electrospun fiber for urethral reconstruction. *International urology and nephrology*, *47*(1), 95-99.

38. Liu, G., Fu, M., Li, F., Fu, W., Zhao, Z., Xia, H., & Niu, Y. (2020). Tissue-engineered PLLA/gelatine nanofibrous scaffold promoting the phenotypic expression of epithelial and smooth muscle cells for urethral reconstruction. *Materials Science and Engineering: C*, *111*, 110810.

39. Lv, X., Guo, Q., Han, F., Chen, C., Ling, C., Chen, W., & Li, B. (2016). Electrospun poly (l-lactide)/poly (ethylene glycol) scaffolds seeded with human amniotic mesenchymal stem cells for urethral epithelium repair. *International Journal of Molecular Sciences*, *17*(8), 1262.

40. Hu, J., Ai, B., Zhu, S., Wang, Z., Xia, H., & Jia, W. (2022). Electrospun PLGA and PLGA/gelatin scaffolds for tubularized urethral replacement: Studies in vitro and in vivo. *Journal of Biomaterials Applications*, *36*(6), 956-964.

41. Sartoneva, R., Haaparanta, A. M., Lahdes-Vasama, T., Mannerström, B., Kellomäki, M., Salomäki, M., ... & Haimi, S. (2012). Characterizing and optimizing poly-L-lactide-co-ε-

caprolactone membranes for urothelial tissue engineering. Journal of The Royal Society Interface, 9(77), 3444-3454.

42. Jiang, S., Xu, Z., Zhao, Y., Yan, L., Zhou, Z., & Gu, G. (2017). Urethral reconstruction using mesothelial cell-seeded autogenous granulation tissue tube: an experimental study in male rabbits. BioMed Research International, 2017.
43. McHale, M. K., Setton, L. A., & Chilkoti, A. (2005). Synthesis and in vitro evaluation of enzymatically cross-linked elastin-like polypeptide gels for cartilaginous tissue repair. *Tissue engineering*, *11*(11-12), 1768-1779.
44. E. S. Sani, A. Kheirkhah, D. Rana, Z. Sun, W. Foulsham, A. Sheikhi, A. Khademhosseini, R. Dana, N. Annabi, Science Advances 2019, 5, eaav1281.
45. E. S. Sani, R. P. Lara, Z. Aldawood, S. H. Bassir, D. Nguyen, A. Kantarci, G. Intini, N. J. M. Annabi, 2019.
46. Yue, K., et al., Structural analysis of photocrosslinkable methacryloyl-modified protein derivatives. Biomaterials, 2017. 139: p. 163-171.
47. Claassen, C., et al., Quantification of Substitution of Gelatin Methacryloyl: Best Practice and Current Pitfalls. Biomacromolecules, 2018. 19(1): p. 42-52.
48. Lee, S., Sani, E. S., Spencer, A. R., Guan, Y., Weiss, A. S., & Annabi, N. (2020). Human□ recombinant□Elastin□based bioinks for 3D bioprinting of vascularized soft tissues. Advanced Materials, 32(45), 2003915.
49. Yin, J., et al., 3D Bioprinting of Low-Concentration Cell-Laden Gelatin Methacrylate (GelMA) Bioinks with a Two-Step Cross-linking Strategy. ACS Appl Mater Interfaces, 2018. 10(8): p. 6849-6857

50. How to prepare aqueous dispersions of Carbopol polymers - lubrizol. (n.d.). Retrieved May 24, 2022, from https://www.lubrizol.com/-/media/Lubrizol/Health/TDS/TDS-61_How_to_Prepare_Aqueous_Dispersions_of_Carbopol.pdf
51. Lei Xu et al 2020 Biofabrication 12 045012 " Bioprinting small diameter blood vessel constructs with an endothelial and smooth muscle cell bilayer in a single step"
52. si, G., Jones, J., Baghdasarian, S., Kaneko, N., Shirzaei Sani, E., Lee, S., ... & Annabi, N. (2021). Engineering elastic sealants based on gelatin and elastin□like polypeptides for endovascular anastomosis. *Bioengineering & translational medicine*, *6*(3), e10240.
53. Datta, P., Ayan, B., & Ozbolat, I. T. (2017). Bioprinting for vascular and vascularized tissue biofabrication. *Acta biomaterialia*, *51*, 1-20.
54. Markiewicz, M. R., Margarone III, J. E., Barbagli, G., & Scannapieco, F. A. (2007). Oral mucosa harvest: an overview of anatomic and biologic considerations. *EAU-EBU update* series, 5(5), 179-187.
55. Zhang, Y. N., Avery, R. K., Vallmajo□Martin, Q., Assmann, A., Vegh, A., Memic, A., ... & Khademhosseini, A. (2015). A highly elastic and rapidly crosslinkable elastin□like polypeptide□based hydrogel for biomedical applications. Advanced functional materials, 25(30), 4814-4826.
56. Shirzaei Sani E, Portillo□Lara R, Spencer A, et al. Engineering adhesive and antimicrobial hyaluronic acid/elastin□like polypeptide hybrid hydrogels for tissue engineering applications. ACS Biomater Sci Eng. 2018;4(7):2528□2540. 10.1021/acsbiomaterials.8b00408

57. Annabi, N., Rana, D., Sani, E. S., Portillo-Lara, R., Gifford, J. L., Fares, M. M., ... & Weiss, A. S. (2017). Engineering a sprayable and elastic hydrogel adhesive with antimicrobial properties for wound healing. Biomaterials, 139, 229-243.